

## Seasonal and intraseasonal biogeochemical variability in the thermocline ridge of the southern tropical Indian Ocean

L. Resplandy,<sup>1</sup> J. Vialard,<sup>1</sup> M. Lévy,<sup>1</sup> O. Aumont,<sup>2</sup> and Y. Dandonneau<sup>1</sup>

Received 18 December 2008; revised 15 May 2009; accepted 20 May 2009; published 23 July 2009.

[1] The Sea-viewing Wide Field-of-view Sensor (SeaWiFS) time series shows high variability of surface chlorophyll at seasonal and intraseasonal time scales in the oligotrophic southern tropical Indian Ocean thermocline ridge called the Seychelles-Chagos thermocline ridge (SCTR). The SCTR is characterized by an open ocean upwelling due to local Ekman pumping, which annually maintains the mixed layer (ML) shallow and is responsive to atmospheric forcing and in particular to the Madden-Julian Oscillation (MJO) at an intraseasonal time scale. Here we present an overview of SCTR biogeochemistry and investigate the physical processes driving the response observed at seasonal and intraseasonal time scales. Using satellite observations and biophysical ocean simulations, we show that seasonal and intraseasonal SeaWiFS signals (in austral winter and during MJO events, respectively) correspond to wind-induced mixing episodes. During such episodes, entrainment fertilizes the ML and allows phytoplankton production. Increased surface production is compensated by a decrease in the subsurface due to light limitation, leading to no significant change in integrated biomass and carbon export. Satellite observations and model results support the conclusion that the biogeochemical response to MJO is highly dependent on interannual variability of thermocline depth. Following Indian Ocean Dipole events, deepened nutrient-rich waters prevent nutrient input into the ML, decreasing the biogeochemical response to MJO. These results shed light on the physical processes at work in the strong surface temperature response to MJO in this region and suggest that entrainment cooling can play a role in the temperature signature to the MJO but is highly modulated by basin-scale interannual variability.

**Citation:** Resplandy, L., J. Vialard, M. Lévy, O. Aumont, and Y. Dandonneau (2009), Seasonal and intraseasonal biogeochemical variability in the thermocline ridge of the southern tropical Indian Ocean, *J. Geophys. Res.*, *114*, C07024, doi:10.1029/2008JC005246.

### 1. Introduction

[2] The most obvious variability in surface chlorophyll (Chl) over the Indian Ocean is associated with the seasonal cycle and the monsoonal reversal of winds north of 10°N. The ecosystem is stratified and near oligotrophic (unproductive) during spring and fall intermonsoons, while intense winds drive convective mixing during the northeast monsoon and coastal upwelling during the southwest monsoon [Banse and English, 1993; Brock and McClain, 1992; Smith *et al.*, 1998; Hood *et al.*, 2003; Wiggert *et al.*, 2000, 2005, 2006; Lévy *et al.*, 2007; Koné *et al.*, 2009]. Another strong contribution to Indian Ocean surface Chl variability is due to interannual variability [Wiggert *et al.*, 2002, 2005; Brock and McClain, 1992], associated either with El Niño remote

forcing or with the Indian Ocean Dipole [Saji *et al.*, 1999; Webster *et al.*, 1999; Murtugudde *et al.*, 2000].

[3] At the intraseasonal scale (~10–90 days), two sources of surface Chl variability are commonly described: small-scale physical features such as eddies and filaments, which are omnipresent mainly in the Arabian Sea and Bay of Bengal [Kawamiya, 2001; Kawamiya and Oschlies, 2003; Prasanna Kumar *et al.*, 2004], and Rossby waves [Cipollini *et al.*, 2001; Kawamiya and Oschlies, 2001; Uz *et al.*, 2001; Dandonneau *et al.*, 2003]. The atmosphere and ocean in the tropics are also strongly affected by another source of intraseasonal variability: the Madden-Julian Oscillation (MJO) (see Madden and Julian [1994] and Zhang [2005] for reviews of this phenomenon).

[4] The MJO is a large-scale intraseasonal perturbation of tropical convection (with most energetic variations at 40–60 days) that develops in the Indian Ocean during austral summer and then propagates eastward into the western Pacific. It is associated with large surface wind and heat flux perturbations driving sea surface temperature (SST) response [Hendon, 2005; Waliser *et al.*, 2003, 2004]. A

<sup>1</sup>LOCEAN-IPSL, IRD, MNHN, UPMC, CNRS, Paris, France.

<sup>2</sup>LPO, IRD, IFREMER, UBO, CNRS, Brest, France.

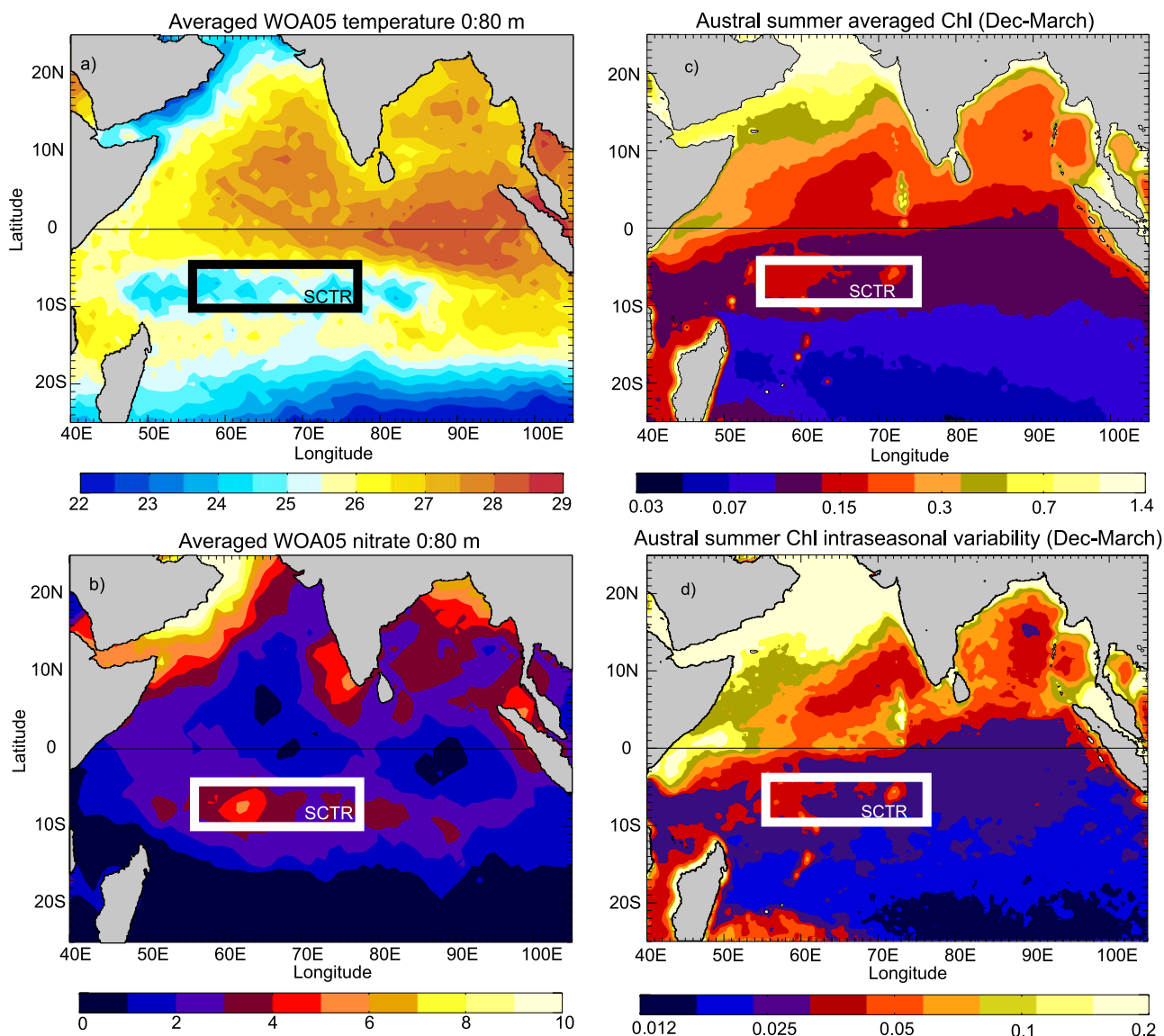


**Figure 1.** Annual WOA05 (a) temperature and (b) nitrate concentration (in  $\text{mmol N m}^{-3}$ ) averaged between the surface and 80 m in the Indian Ocean. (c) SeaWiFS seasonal mean during austral summer (December–March) ( $\text{mg m}^{-3}$ ). (d) Intraseasonal variability of SeaWiFS Chl during austral summer estimated by the averaged RMS of  $(\text{Chl} - \text{Chl}^*)$  between December and March of years 1998–2007.

Here  $\text{Chl}^*$  is the 2 month sliding average. More exactly, we plot in each point  $\log \left[ \sqrt{\frac{1}{n} \sum_{i=0}^n (\text{Chl} - \text{Chl}^*)^2} \right]$ , with  $n$  being the number of samples in the time series (10 years with 15 samples between December and March,  $n = 10 \times 15 = 150$ ). This method corresponds to a 16–60 day high-pass filter. The rectangle corresponds to the domain of study, called the SCTR box (55–75°E, 5–10°S). Note that spots of high values correspond to the Seychelles Archipelago and the Chagos Archipelago.

recent analysis of satellite Chl concentrations also suggests that MJO wind-induced mixing drives a response of surface Chl at a large scale, especially in the North Indian Ocean and the tropical Pacific Ocean [Waliser *et al.*, 2005].

[5] One of the regions of strongest SST signals associated with the MJO is the 5–10°S band in the Indian Ocean [Harrison and Vecchi, 2001; Duvel *et al.*, 2004; Saji *et al.*, 2006; Duvel and Vialard, 2007; Vinayachandran and Saji, 2008; Vialard *et al.*, 2009]. This region, recently described by Hermes and Reason [2008] as the Seychelles-Chagos

thermocline ridge (SCTR), is characterized by strong Ekman pumping due to the northward weakening of the southeast trades [e.g., McCreary *et al.*, 1993]. The resulting shallow thermocline centered around 8°S is comparable in depth to the one in the eastern Pacific equatorial upwelling and can be easily identified in Figure 1a, which shows the temperature averaged between the surface and 80 m over the Indian Ocean. Moreover, this latitudinal band of shallow thermocline is associated with shallow nutrient-rich waters (Figure 1b). Within the thermocline ridge, we focus on the

SCTR, defined here as the region between 55 and 75°E (see rectangle in Figure 1), where the thermocline and the nutrient-rich waters are the shallowest.

[6] Despite the presence of an open ocean upwelling that can be identified as a maximum in Chl observed by the Sea-viewing Wide Field-of-view Sensor (SeaWiFS) (Figure 1c) [Lévy *et al.*, 2007; Xie *et al.*, 2002], there is to our knowledge no work that addresses the implication of this upwelling on the biogeochemical seasonal cycle in the SCTR region. Moreover, the SCTR gathers most of the ingredients for surface blooms during austral summer MJO events: a shallow mixed layer (ML) that allows photosynthesis, a shallow thermocline associated with shallow nutrient-rich waters (Figures 1a and 1b) and strong wind variations. This is supported by the presence of an open ocean maximum in intraseasonal variability of surface Chl observed by SeaWiFS (Figure 1b). Chl variability in response to the MJO in this region was recently reported by Vinayachandran and Saji [2008]. They hypothesize that it is due to the entrainment of Chl from the deep chlorophyll maximum as is the case for Rossby waves propagation farther east [Kawamiya and Oschlies, 2001].

[7] Using a combination of satellite data, climatological data, and coupled physical-biogeochemical ocean simulations, we investigate the biogeochemical variability in the SCTR at two time scales. First, we describe the seasonal cycle associated with the open ocean upwelling regime, which is essential to properly understand the response at other time scales. Then, we present the processes at play in intraseasonal variability due to the MJO. The model is also used to estimate the impact of biogeochemical seasonal and intraseasonal variability on the carbon export, which is not validated since no data are available in the region.

[8] The SCTR is also known as a region of strong interannual variability of the thermocline depth [Masumoto and Meyers, 1998]. This variability seems to be largely the result of the Indian Ocean Dipole [Webster *et al.*, 1999], while El Niño forces thermocline variability farther south [Rao and Behera, 2005; Yu *et al.*, 2005]. Several studies have suggested that interannual variability of the thermocline in this region might modulate the SST signature of the MJO [e.g., Harrison and Vecchi, 1999; Duvel and Vialard, 2007; Vialard *et al.*, 2009]. We will investigate if interannual variability of the thermocline in the SCTR also modulates the Chl response to MJO.

[9] The content is organized as follows. In section 2, we describe the data and the model used in this study. The biogeochemical seasonal variability is described from observations and model results in section 3. Section 4 presents the biogeochemical response to two particular MJO events. In section 5, we investigate how interannual variability modulates the amplitude of the Chl response to MJO. Finally, main findings and conclusions are given in section 6.

## 2. Model and Data

### 2.1. Model

[10] The physical ocean model used in this study is the ORCA05 global configuration of the ocean general circulation model NEMO [Madec, 2008]. The model has a mean horizontal resolution of 0.5° and 30 vertical levels increasing from 10 m at the surface to 500 m at depth. The lateral

diffusion is oriented along the isopycnals, and the eddy parametrization scheme of Gent and McWilliams [1990] is applied poleward of 10°S and 10°N. The reader is referred to the work of de Boyer Montégut *et al.* [2007] for a more complete description of the physical model.

[11] The ocean general circulation model is coupled with the ocean biogeochemical model Pelagic Interaction Scheme for Carbon and Ecosystem Studies (PISCES). PISCES was successfully used to simulate the biogeochemical fields in the global ocean and to understand their dynamics [Aumont *et al.*, 2003; Aumont and Bopp, 2006]. The model includes 24 compartments. Phytoplankton (PHY) growth can be limited by five nutrients: nitrate (NO<sub>3</sub>), ammonium (NH<sub>4</sub>), phosphate, silicate, and iron (Fe). Four living pools are represented: two phytoplankton size classes (nanophytoplankton and diatoms) and two zooplankton size classes (microzooplankton and mesozooplankton). For all living compartments, the ratios among carbon (C), nitrogen (N), and phosphorus (P) are kept constant to the values proposed by Takahashi *et al.* [1985]. The internal contents in Fe of both phytoplankton groups and in silicon (Si) of diatoms are prognostically simulated as a function of the external concentrations in nutrients and the light level. All the elemental ratios of zooplankton are kept constant. PISCES contains three nonliving compartments: semilabile dissolved organic matter and slow (3 m d<sup>-1</sup>) and fast (50–200 m d<sup>-1</sup>) sinking particles. As for the living compartments, constant Redfield ratios are imposed for C:N:P. However, Fe, Si, and calcite in particles are fully simulated. We estimated the carbon export by calculating the carbon content of the two size classes of particles sinking across a given depth. Fe deposition from the atmosphere has been estimated from climatological monthly maps of dust deposition simulated by the LMDzT-INCA model [Balkanski *et al.*, 2004]. Monthly river discharge of carbon is taken from the global erosion model of Ludwig *et al.* [1996]. Fe, N, P, and Si supplies are derived from the same model with constant Fe:P:N:Si:C ratios. Fe mobilization is simulated using a constant source modulated by a factor computed from the metamodel of Middelburg *et al.* [1996].

### 2.2. Model Run

[12] The physical model NEMO has been initialized from rest with salinity and temperature climatologies of the World Ocean Atlas 2001. The biogeochemical model is initialized from output of a NEMO-PISCES 3000 year spin-up simulation at 2° resolution [see Aumont and Bopp, 2006]. The model is driven by daily wind stress, atmospheric air temperature, and wind speed from the European Centre for Medium-Range Weather Forecasts 40 year re-analysis (ERA-40) [Uppala *et al.*, 2005]. Monthly precipitation is taken from the Common Ocean-ice Reference Experiments (CORE) data set [Large and Yeager, 2004]. To avoid any strong model drift, modeled sea surface salinity is restored to the monthly World Ocean Atlas 2001 data set [Conkright *et al.*, 2002] with a time scale of about 40 days. Climatological monthly relative humidity [Trenberth *et al.*, 1989] and cloud cover [Rossow and Schiffer, 1999] are applied over the course of the simulation. Surface heat fluxes and evaporation were computed using empirical bulk formulae described by Goose [1997]. An

interannual simulation is performed over 1958–2001 starting from this spin-up and using the same forcing fields.

### 2.3. Model-Derived Chl

[13] Chl in the model is calculated from the carbon content of both PHY size classes through a variable Chl:C ratio. The Chl:C ratio is modeled using a modified version of the photoadaptation model by *Geider et al.* [1998]. Unless specified, model Chl in this study represents the pigment concentration averaged in the SCTR box (55–75°E, 5–10°S; see rectangle in Figure 1) between the surface and the optical depth. The optical depth is calculated as the depth where the solar radiation is equal to the radiation at the surface divided by  $e$ , which takes into account the attenuation due to the water and phytoplankton.

### 2.4. Chl Data

[14] Level 3 standard-processed 8-day composite 9 km × 9 km SeaWiFS surface Chl  $a$  were used to validate the model Chl section 2.3. Data were processed using NASA's SeaWiFS Data Analysis System (SeaDAS) software package. To describe the seasonal cycle, we used a 7-year climatology (April 1998 to March 2005) available at <http://www.nio.org> [*Lévy et al.*, 2007]. Estimating the intra-seasonal Chl signal associated with the MJO in SeaWiFS data is difficult because of missing data due to clouds. The MJO is indeed characterized by a strong modulation of tropical convection, and clouds prevent satellite detection of the Chl (see Figures 6a–6c). Fortunately, during MJO the wind increase that is likely to promote a Chl response is often shifted west of the convection maximum [e.g., *Duvel and Vialard*, 2007]. To evaluate the uncertainty associated with the missing pixels, we estimated the spatial variability within the SCTR box (55–75°E, 5–10°S; see rectangle in Figure 1) for each SeaWiFS 8-day composite by using the upper and lower quartiles of the Chl distribution inside the box. A large spread of these two values indicates a potentially large error on the estimated mean. We used quantiles rather than standard deviation or a classical significance interval because it suits the highly nonnormal nature of the Chl values distribution better.

### 2.5. MJO Index

[15] *Wheeler and Hendon* [2004] have developed an index to monitor MJO activity in all seasons in the tropics. We use this index to determine if active MJO conditions are present over the SCTR. For that, we select austral summer events with amplitude larger than 1 during phases 2, 3, and 4 (which designate active MJO phases with largest surface wind response over the SCTR). We added an additional criterion for wind speed ( $\geq 7 \text{ m s}^{-1}$ ) because it is the main driving factor for the upper ocean response: while the MJO active phase sets the stage for increased convection and surface wind speed, the timing of the local wind increase in the SCTR depends on the exact pattern of convective anomaly and may vary from one event to another [*Duvel and Vialard*, 2007].

## 3. Seasonal Variability in the SCTR Region

### 3.1. Driving Factors of Chl Seasonal Variability

[16] Figure 2a shows the seasonal cycle of two key parameters forcing the biogeochemical model and control-

ing phytoplankton growth: ERA-40 wind speed that modulates mixing of nutrients and phytoplankton and incoming shortwave (SW) radiation. ERA-40 winds in the region display a typical monsoon winter-summer reversal. Austral summer months are characterized by weak northwesterly winds, while austral winter months are characterized by intense southeast trade winds that remain quite strong through fall and spring intermonsoons. The temporal evolution of the mixed layer depth (MLD) based on observations (dashed line in Figure 2b) follows the wind forcing; it varies between 25 m in December–March and 50 m in August. The SW radiation annual cycle is mainly driven by the seasonal movements of the Sun (solid line in Figure 2a); during austral summer it peaks around  $210 \text{ W m}^{-2}$ , while during austral winter it drops to  $160 \text{ W m}^{-2}$ . SW radiation is slightly modulated during austral summer by an increased cloud cover in December–January.

[17] World Ocean Atlas 2005 (WOA05) temperature (Figure 2b) and nitrate (Figure 2c) vertical profiles display a semiannual cycle associated with the Ekman pumping seasonal cycle. As reported by *Yokoi et al.* [2008], both the 20°C isotherm and the nutricline (estimated here as the nitrate  $2.4 \text{ mmol m}^{-3}$  isopleth) are shallow in December–January and May–June and reach maximum depths in March and October. Temperature and nitrate vertical distributions in the model (Figures 2d and 2e) are comparable to WOA05 profiles (Figures 2b and 2c). The model slightly underestimates the upwelling in May–June when compared to WOA05 data, which reduces the seasonal variation of the 20°C isotherm (15 m in the model versus 20 m in the WOA05) and the nutricline. Temperature profile variations in the model are, however, consistent with previous modeling work in this region [*Schott and McCreary*, 2001; *Hermes and Reason*, 2008]. Note that abrupt changes in nitrate WOA05 climatology in May and October are derived from coarse resolution observations (70 data points on average between 0 and 100 m, whereas other months are derived from 230 data points on average). The resulting amplitude of WOA05 nutricline variations is most likely exaggerated.

[18] WOA05 Chl data available in the region (not shown) are at very coarse spatial and temporal resolution and do not allow a satisfying description of the seasonal cycle. The best coverage available is provided by SeaWiFS surface Chl observations. SeaWiFS data (solid line in Figure 2f) reveal an annual Chl increase in the surface layer during austral winter (June–August). Simulated Chl above the optical depth is very similar to SeaWiFS observations, and the austral winter peak is well resolved in both timing and amplitude (Figure 2f).

[19] Surface Chl in the model follows the surface concentration in nitrogen nutrients (nitrate plus ammonium) that increases between May and August (Figure 2g) following the ML deepening associated with austral summer winds. The positive Ekman pumping that upwells shallow nutrient-rich waters in the SCTR (see integrated  $\text{NO}_3$  between 0 and 80 m in Figure 1b) enhances the effect of wind-driven mixing and favors nutrients input to the surface.

### 3.2. Biogeochemical Seasonal Variability

[20] In this section, we present some model diagnostics that bring insight to the biogeochemical processes in the

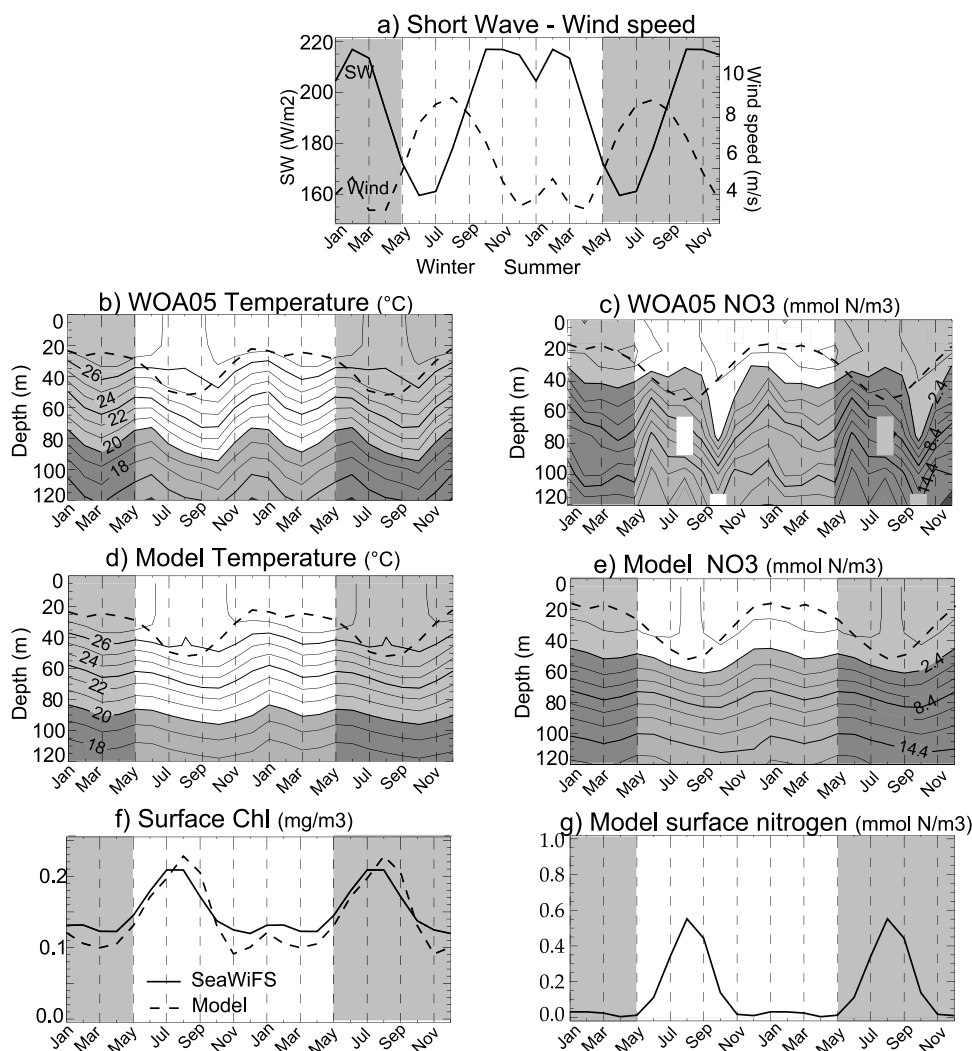


**Figure 2.** Monthly climatology of (a) ERA-40 wind speed ( $\text{m s}^{-1}$ ) (solid line) and CORE shortwave (SW) radiation ( $\text{W m}^{-2}$ ) (dashed line), (b) WOA05 temperature profile, (c) WOA05 nitrate concentration profile ( $\text{NO}_3$ ,  $\text{mmol N m}^{-3}$ ), (d) model temperature profile, (e) model nitrate concentration profile ( $\text{NO}_3$ ,  $\text{mmol N m}^{-3}$ ), (f) surface Chl concentration observed by SeaWiFS (solid line) and in the model averaged between the surface and the optical depth (dashed line), and (g) surface model nitrogen equal to the sum of model nitrate and ammonium concentrations ( $\text{mmol N m}^{-3}$ ). A  $2^\circ$  resolution climatology of the MLD (dashed line) derived from individual profiles (available at <http://www.lodyc.jussieu.fr/~cdblod/mld.html>) [de Boyer Montégut et al., 2004] is superimposed in Figures 2b and 2d. Model MLD is superimposed with model results in Figures 2d and 2e.

region. The diagnostic of carbon export is more speculative since it could not be validated because of the lack of data. Figure 3 shows the photosynthetically available radiation (PAR) profile that gives the light that actually penetrates the water column (Figure 3a), PHY biomass (concentration profile in Figure 3b and integration over the first 25 and 100 m in Figure 3c) and carbon export at 25 and 100 m (Figure 3d).

[21] During austral summer, the averaged MLD ( $\sim 20$  m) is shallower than the nutricline ( $\sim 40$  m), therefore greatly reducing nutrients input in the surface layer (Figures 2e and 2g); PHY is mainly located at subsurface depths around 60 m (Figure 3b) where nutrients are available (Figures 2c and 2e). The annual surface Chl peak that starts in May (Figure 2f) is correlated with an increase in PHY in surface

waters and a decrease at the subsurface (Figure 3b). As explained in section 3.1, PHY growth at the surface is triggered by the deepening of the ML due to intense winter winds that enriches surface waters with nutrients. At the same time, PHY at the subsurface drastically decreases with the diminution of PAR (Figure 3a) because of the combination of decreased SW radiation (Figure 2a) and autoshading related to the presence of PHY at the surface. Toward the end of austral winter, surface PHY starts decreasing with the water column restratification and nutrient depletion (Figure 2g).

[22] Opposite variations between the surface and subsurface in the PHY seasonal cycle roughly compensate, and the integrated PHY between the surface and 100 m remains quite stable around  $115 \text{ mmol C m}^{-2}$  (Figure 3c). As a

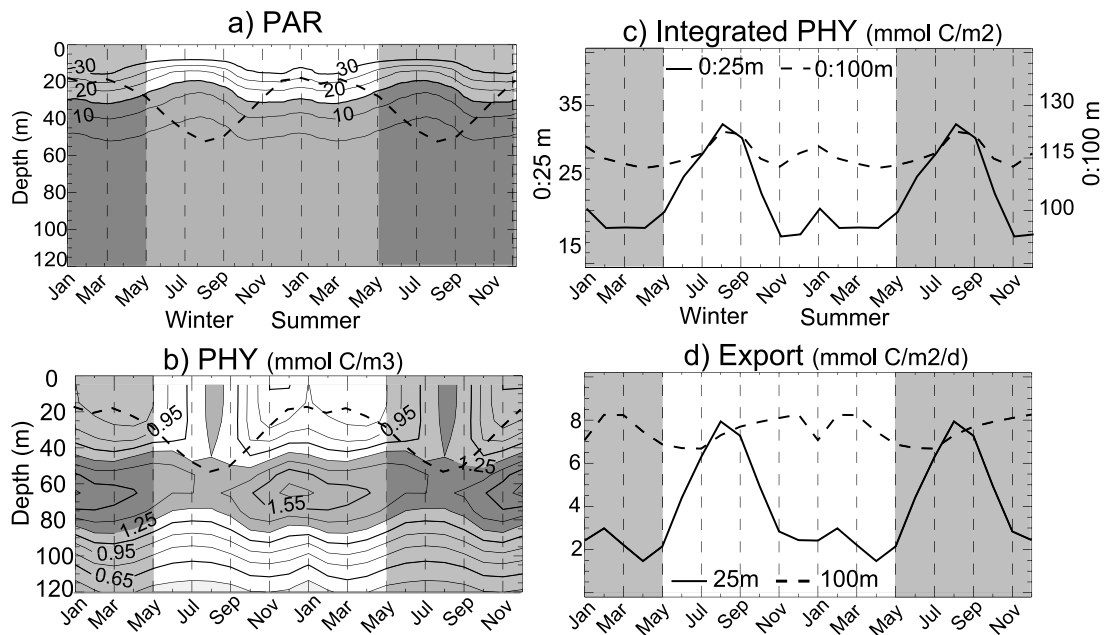


**Figure 3.** Model monthly climatology of (a) photosynthetically available radiation (PAR) ( $\text{W m}^{-2}$ ) and (b) phytoplankton concentration ( $\text{mmol C m}^{-3}$ ) (contours) superimposed with MLD (dashed line); (c) integrated phytoplankton ( $\text{mmol C m}^{-2}$ ) between the surface and 25 m (solid line, left axis) and between the surface and 100 m (dashed line, right axis); and (d) carbon export, which corresponds to the carbon content of the two size classes of organic matter particles ( $\text{mmol C m}^{-2} \text{d}^{-1}$ ) sinking across 25 m depth (solid line) and 100 m depth (dashed line).

consequence, the seasonal variability of carbon export associated with the PHY seasonal cycle that is predicted by the model at 25 m is damped, and no strong seasonality is detected at 100 m (Figure 3d).

#### 4. Intraseasonal Response of Chl During 2000 and 2001 MJO Events

[23] Climatological surface Chl from SeaWiFS displays an increase during austral winter and a flat signal during austral summer (Figure 2f). However, events of surface Chl in austral summer significantly higher than climatological values appear from the SeaWiFS interannual time series. Figures 4 and 5 focus on two remarkably strong events between October 1999 and December 2001. During events labeled MJ1 and MJ2, SeaWiFS Chl concentration (solid blue line) reaches about twice the climatological concentration ( $0.1 \text{ mg m}^{-3}$ , dashed blue line) and is similar to typical winter peak values. The MJO index developed by *Wheeler and Hendon* [2004] confirms that these two episodes are associated with an MJO active phase over the Indian Ocean (blue line in Figure 4b).

[24] Figure 6 shows snapshots of Chl during MJ2 in SeaWiFS observations and in the model. Despite the intense cloud coverage in SeaWiFS images, it is clear that the surface Chl increases remarkably during MJ2. The number of available Chl pixels (not shown) used in Figures 4 and 5 indicates clearly that during MJ1 and MJ2, the increased atmospheric convection is associated with a poor sampling of the area of interest. However, the highest and lowest quartiles of the Chl in the SCTR box (grey shading in Figure 4a) suggest that during MJ1 and MJ2, the Chl peak is

significant. Indeed, even the threshold value of the lowest quartiles of surface Chl raises clearly above the value before the convective and wind events.

[25] Surface Chl temporal evolution in the model is similar to SeaWiFS observations (Figure 4a). The amplitude and timing of the surface Chl increase during MJ1 and MJ2 are well reproduced. Moreover, MJ1 and MJ2 Chl peaks identified in the SeaWiFS time series correspond to a wide Chl pattern covering the entire region, which is comparable in both the model and the data (Figure 6).

[26] Comparison of Figures 4a and 4b highlights the correlation between these surface Chl peaks and wind bursts associated with MJOs with intensity that reaches typical winter values ( $\geq 7 \text{ m s}^{-1}$ ). Two hypotheses could explain the Chl signature observed by SeaWiFS: (1) Chl is produced at the surface because phytoplankton growth is allowed by nutrient input as suggested by *Waliser et al.* [2005] or (2) Chl produced in the subsurface is entrained to the surface as suggested by *Vinayachandran and Saji* [2008].

[27] Figures 5a–5c show the temporal evolution of Chl, nitrate, and PHY profiles in the model superimposed with the MLD. Before MJ1 and MJ2 the ML is shallow ( $\sim 15 \text{ m}$ ) and depresses nutrient input to the surface by mixing. The surface is therefore highly oligotrophic, and phytoplankton concentration is low. During MJ1 and MJ2, strong wind bursts deepen the ML to 25 m.

[28] We made a rough estimation of the Chl entrained by mixing during MJ1 and MJ2. During MJ1 the MLD reaches 25 m, with a concentration of Chl  $\sim 0.17 \text{ mg m}^{-3}$  (Figure 5a). Right before MJ1, the MLD is 15 m, with a concentration of  $0.02 \text{ mg m}^{-3}$ . If we integrate Chl over the first 25 m just before MJ1 (maximum depth reached by the MLD during

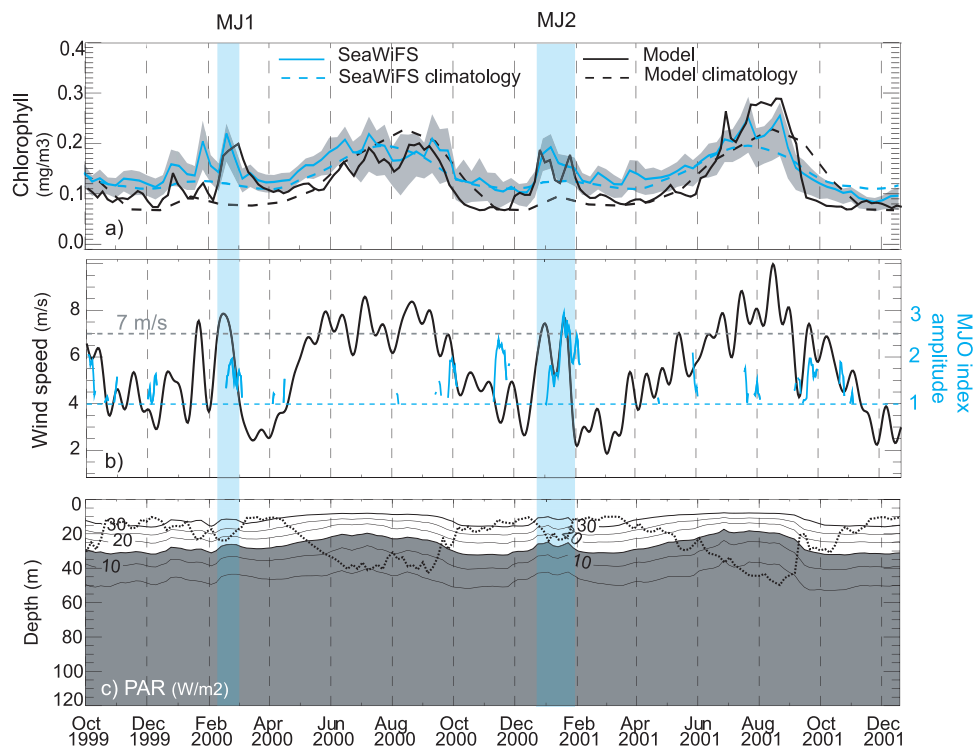


**Figure 4.** October 1999 to December 2001 time series of (a) surface SeaWiFS Chl median (solid blue line) over the domain superimposed with the first and third quartile interval (grey shading) compared with model Chl averaged between the surface and the optical depth (solid black line) and model (dashed black line) climatologies are also shown. (b) ERA-40 wind speed (solid black line,  $\text{m s}^{-1}$ ) and *Wheeler and Hendon* [2004] MJO index amplitude (blue line). Only MJOs in phases 2, 3, or 4 with an amplitude  $\geq 1$  and occurring during austral summer are shown [*Wheeler and Hendon*, 2004]. (c) Photosynthetically available radiation ( $\text{W m}^{-2}$ ) superimposed with model MLD (dashed black line). Events highlighted in blue (MJ1 and MJ2) correspond to an active MJO phase over the Indian Ocean with amplitude  $\geq 1$  and wind speed  $\geq 7 \text{ m s}^{-1}$ .

MJ1), we obtain an average concentration of  $\sim 0.06 \text{ mg m}^{-3}$ , which is lower than the concentration observed during MJ1. Similarly, for MJ2 we obtained an average concentration of  $\sim 0.07 \text{ mg m}^{-3}$ , which is lower than the  $0.15 \text{ mg m}^{-3}$  observed. The Chl signal associated with MJO cannot be explained by mixing alone and corresponds to biomass produced at the surface. This is supported by model results that show an increase in nutrient and PHY concentration at the surface. During MJ1 and MJ2 the ML deepens fertilizing surface waters with nitrate (Figure 5b) and ammonium (not shown) but remains shallow enough to allow phytoplankton growth (Figure 5c). PHY response lasts about a month and decreases rapidly toward the end of MJO wind bursts because of prompt restratification and nutrient depletion at the surface.

[29] It is interesting to note that the increase in integrated PHY between the surface and 25 m during MJ1 and MJ2 ( $\sim 25\%$ , solid line in Figure 5d) is partly counterbalanced by a decrease in subsurface concentration (Figure 5c) as was the case at the seasonal time scale (see section 3.2). This can be explained by the decrease in ML PAR (Figure 4c) due to auto shading related to surface PHY increase during MJO. The carbon export at 25 m increases during MJ1 and MJ2 ( $\sim 50\text{--}100\%$ ), but the compensation of PHY production between the surface and subsurface damps intraseasonal variability of the export at 100 m (Figure 5e). As a result,

the signature of MJO events on integrated PHY biomass (dashed line in Figure 5d) and carbon export below the subsurface (dashed line in Figure 5e) remains small ( $\leq 10\%$ ).

## 5. Interannual Modulation of Chl Response to MJO

[30] Section 4 focused on the biogeochemical response to MJO during two particular events. Here we present the interannual variability of this response recorded by SeaWiFS between 1998 and 2007. Using QuikSCAT and MJO index time series (Figures 7b and 7d), eight MJO events (labeled MJ1 to MJ8) of wind intensity  $\geq 7 \text{ m s}^{-1}$  can be identified (see section 2 for the method). Within these events of similar wind intensity ( $7\text{--}9 \text{ m s}^{-1}$ ), SeaWiFS Chl intraseasonal response displays a strong interannual variability (Figure 7a). Only four of the selected MJO events (MJ1, MJ2, MJ3, and MJ5, highlighted in blue) are associated with a significant increase in surface Chl ( $\geq 50\%$ ).

[31] Previous work in the region related the SST response to the MJO to the sea level anomalies (SLA). Positive SLA are associated with a deeper thermocline and less MJO-reactive ML, while negative SLA are characterized by a shallower thermocline and thus much more MJO-reactive

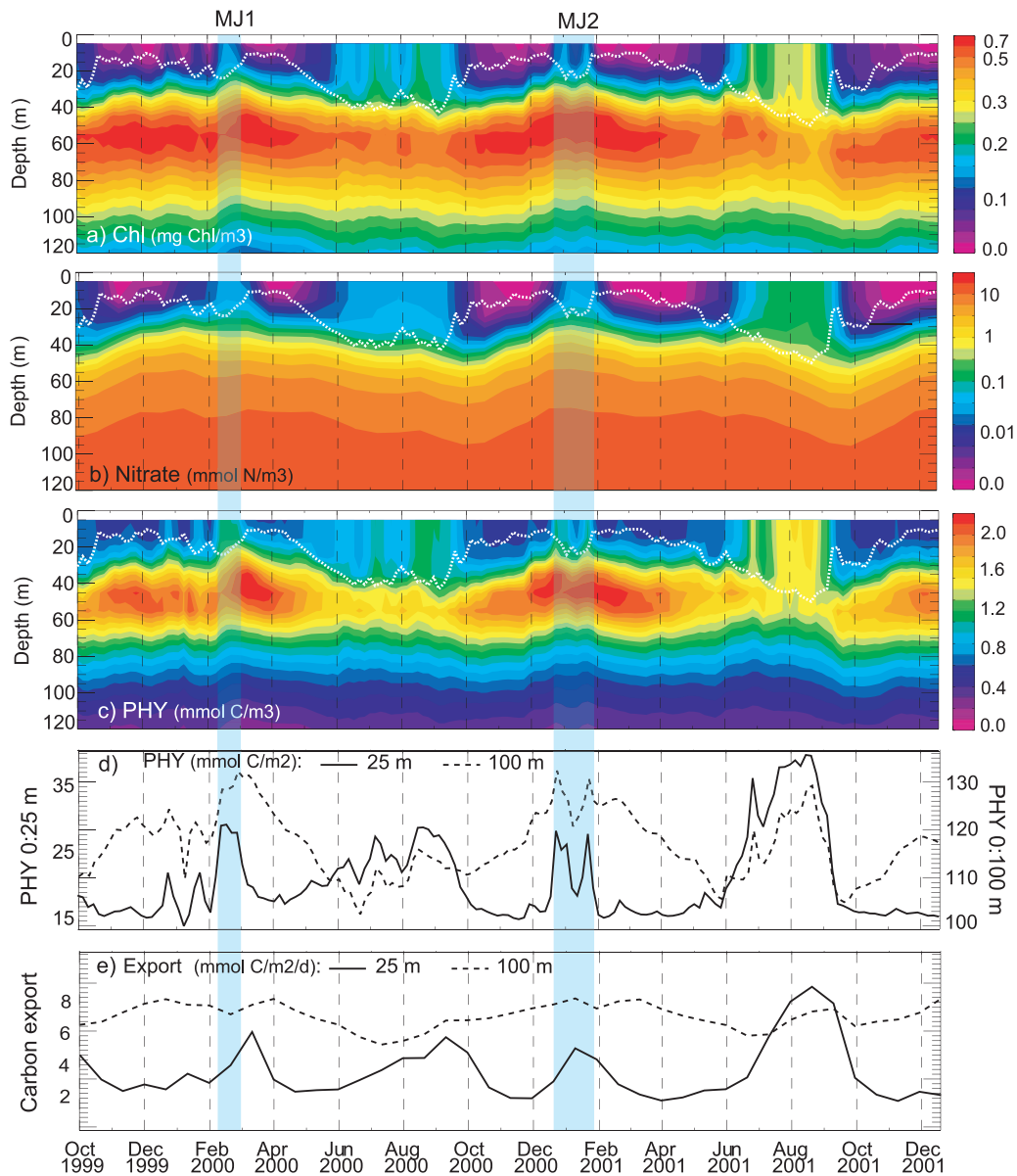


**Figure 5.** October 1999 to December 2001 time series showing model vertical distribution of (a) Chl ( $\text{mg Chl m}^{-3}$ ), (b) nitrates ( $\text{mmol N m}^{-3}$ ), and (c) phytoplankton ( $\text{mmol C m}^{-3}$ ) superimposed with model MLD (dotted white line). (d) Integrated phytoplankton between the surface and 25 m ( $\text{mmol C m}^{-2}$ , solid line and left axis) and between the surface and 100 m ( $\text{mmol C m}^{-2}$ , dashed line and right axis). (e) Carbon export ( $\text{mmol C m}^{-2} \text{d}^{-1}$ ) at 25 m (solid line) and at 100 m (dashed line). Events highlighted in blue (MJ1 and MJ2) correspond to an active MJO phase over the Indian Ocean with amplitude  $\geq 1$  and wind speed  $\geq 7 \text{ m s}^{-1}$  (see Figure 4 and *Wheeler and Hendon [2004]*). Note that the differences in patterns between nitrate and the other variables can be explained by the difference in temporal resolution of model outputs (20 days for nitrate versus 5 days for other variables).



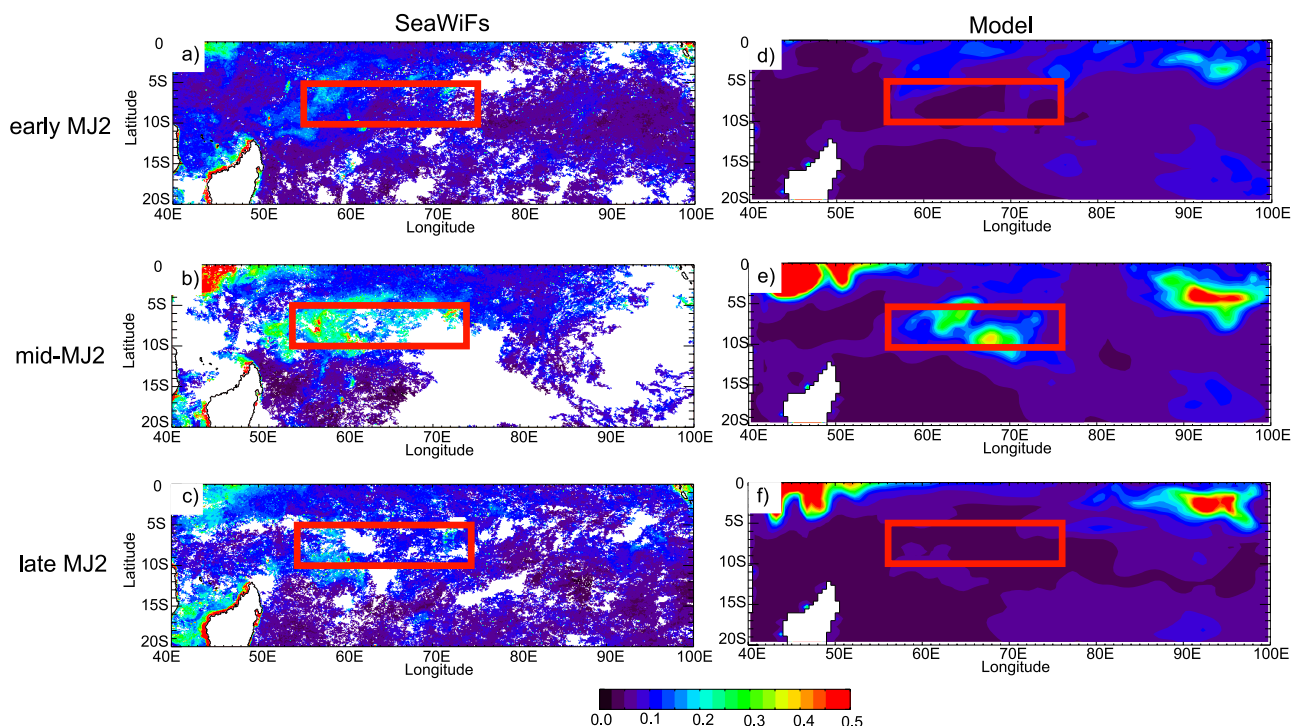


**Figure 6.** Snapshots of surface Chl (in  $\text{mg m}^{-3}$ ) during MJ2 (a–c) from SeaWiFS observations and (d–f) in the model. Figures 6a and 6d are from 22 December 2000; Figures 6b and 6e are from 12 January 2001; and Figures 6c and 6f are from 21 February 2001.

ML [Vialard *et al.*, 2009]. Comparison of SLA and SeaWiFS Chl time series gives similar results to those found for SST response (Figures 7a and 7c). Although the record is short, surface Chl intraseasonal response to the MJO seems to be correlated to SLA; nonresponsive events MJ4, MJ6, MJ7, and MJ8 are associated with positive SLA  $\geq 10$  cm; responsive events MJ1, MJ2, and MJ3 are associated with slightly negative SLA; and finally, during MJ5 the SLA are quite high (0–7 cm), but the Chl peak occurs when the SLA decrease.

[32] We showed in section 4 that the biogeochemical response to MJ1 and MJ2 is triggered by the entrainment of nutrients into the ML. This process is highly facilitated by the particularly shallow position of nutrient isopleth during austral summer. The water column stratification is a key factor in controlling the amplitude of the surface Chl response to the MJO. To confirm the role of stratification on Chl response, we used model results between 1980 and 2001, which allows for investigation of the SLA–intraseasonal Chl response with a larger sample. Chl intraseasonal variability was estimated at each time  $t$ ; we used the standard deviation of band-pass-filtered Chl (10–70 days) in an 80 day window centered on  $t$ . Water column stratification is estimated using the thermocline depth anomaly. Figure 8 is a scatterplot of Chl intraseasonal variability versus thermocline anomaly in the model during austral summer. The thermocline depth is estimated as the depth where vertical stratification (i.e.,  $\partial\rho/\partial z$ , where  $\rho$  is the density) is maximum. The thermocline anomaly and surface Chl intraseasonal variability are correlated; positive anomalies of the thermocline are associated with very low values of Chl intraseasonal variability. In contrast, negative anomalies are mainly associated with relatively high intraseasonal

variability of Chl. The spread of the Chl intraseasonal response for an anomalously shallow thermocline can be explained by the fact that a shallow thermocline is a necessary but not sufficient condition for having a surface Chl response; i.e., there can be a shallow thermocline associated with a shallow nutricline favorable to phytoplankton growth at the surface, but the biological response will occur only in cases where an active MJO over the Indian Ocean induces strong winds over the SCTR.

[33] As mentioned in section 1, the interannual variability of the thermal/haline stratification in the SCTR is mainly due to the Indian Ocean Dipole. The zonal wind anomalies at the equator associated with the Indian Ocean Dipole induce a strong Ekman pumping south of the equator in the central and eastern Indian Ocean. This creates a strong deepening of the thermocline between 5 and 12°S, which later propagates westward under the effect of planetary wave dynamics [e.g., Masumoto and Meyers, 1998; Webster *et al.*, 1999] and affects the SCTR. There is also a similar response associated with El Niño events, but it is located farther south and influences the SCTR less [Rao and Behera, 2005; Yu *et al.*, 2005].

## 6. Conclusion

[34] In the SCTR the biomass is mainly produced in the subsurface where nutrients and light are available. At the surface, low Chl concentrations are modulated at seasonal and intraseasonal scales by very similar processes. The shallow position of the thermocline in the region plays a major role by maintaining the ML at shallow depth and keeping it very responsive to atmospheric and subsurface forcing [e.g., Harrison and Vecchi, 2001; Duvel *et al.*, 2004;

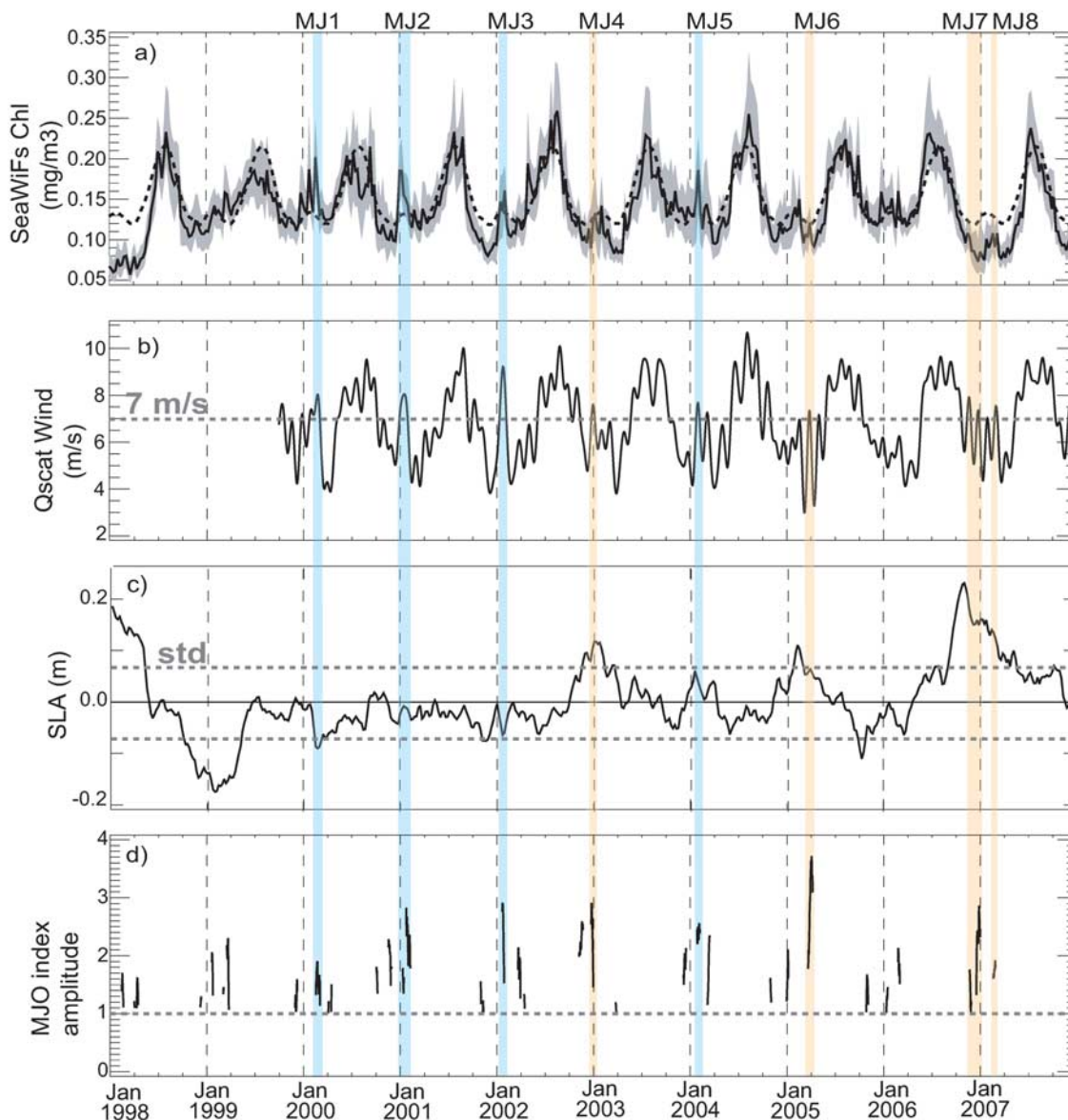


**Figure 7.** January 1998 to December 2007 time series averaged over the SCTR region. (a) Surface SeaWiFS Chl median (black line) over the domain superimposed by 1998–2005 SeaWiFS climatology (dashed line) and the first to third quartile interval (grey shading). The highest and lowest quartiles of the SeaWiFS Chl are used to estimate the uncertainty on the mean due to cloud missing values. (b) QuikSCAT wind speed ( $\text{m s}^{-1}$ ). (c) Sea level anomalies (SLA) (m). (d) *Wheeler and Hendon* [2004] MJO index amplitude. Only MJOs in phases 2, 3, or 4 with an amplitude  $\geq 1$  and occurring during austral summer are shown. Highlighted MJOs correspond to active MJO phases over the Indian Ocean with amplitude  $\geq 1$  and wind speed  $\geq 7 \text{ m s}^{-1}$ ; blue indicates events with a response in Chl, while orange indicates events with no response in Chl.

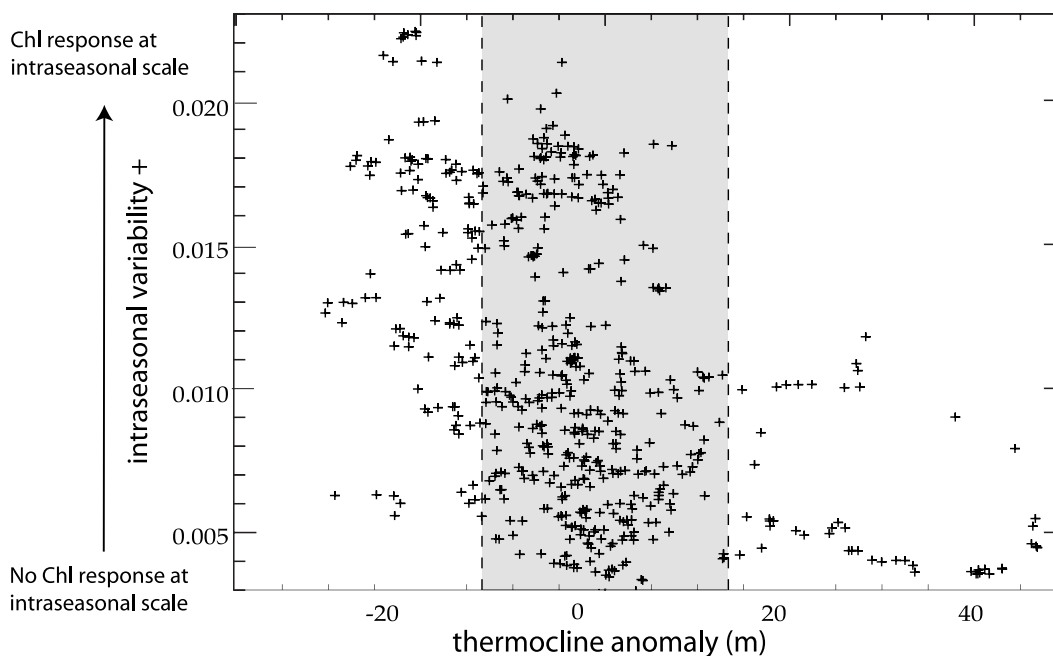


**Figure 8.** Scatterplot of thermocline anomaly (in m) and intraseasonal variability of model surface Chl (in  $\text{mg m}^{-3}$ ) in the SCTR region during austral summer. Note that the thermocline depth is estimated as the depth where vertical stratification (i.e.,  $\partial\rho/\partial z$ , with  $\rho$  as the density) is maximum. The shaded area represents thermocline anomaly standard deviation.

*Duvel and Vialard, 2007*]. The reduced heat content of the ML allows the surface temperature to change quickly. Similarly, the input of subsurface nutrients will be concentrated in a thin layer and will favor phytoplankton production. The intensification of winds in winter and during MJOs triggers the deepening of the ML. The surface Chl increase observed in both cases results from the entrainment of nutrients and the production of phytoplankton in the ML and not only from the entrainment of Chl produced in the subsurface. Our results therefore suggest different processes for the intraseasonal Chl increase in response to the MJO than those suggested by *Vinayachandran and Saji [2008]*.

[35] Our model suggests that when production is triggered at the surface, subsurface production is decreased because of a balance between nutrient and light limitations. Consequently, periods of phytoplankton growth at the surface and subsurface are in phase opposition, predicting weak seasonal and intraseasonal variability of integrated phytoplankton and of carbon export below 100 m.

[36] Our results also indicate that similar to SST, the intensity of the phytoplankton response to the MJO is highly modulated by the interannual variability in thermocline depth. A shallow thermocline associated with shallow nutrient-rich waters and ML is very responsive to intraseasonal wind bursts, while a deep thermocline mainly forced by Indian Ocean dipoles is associated with a deeper nutricline that limits nutrient input into the ML.

[37] The present work does not only help to elucidate biogeochemical processes in the SCTR region but also brings useful information about which physical processes are at work to explain the SST response to the MJO. There is indeed a debate between studies suggesting that entrainment and/or upwelling play a strong role [e.g., *Harrison and Vecchi, 2001; Saji et al., 2006; Vinayachandran and*

*Saji, 2008; I. D. Lloyd and G. A. Vecchi, Submonthly Indian Ocean cooling events and their interaction with large-scale conditions, submitted to *Journal of Climate*, 2009*] and those suggesting that heat flux forcing (reduced shortwave and larger evaporation during active MJO phases) dominates [*Duvel and Vialard, 2007; Vialard et al., 2008*]. An apparent paradox arises when comparing recent studies that convincingly demonstrate that entrainment and Ekman pumping are clearly not negligible for some events [*Vinayachandran and Saji, 2008; I. D. Lloyd and G. A. Vecchi, submitted manuscript, 2009*] and a case study using direct observations from the SCTR that concludes that atmospheric heat fluxes were the dominant processes in late 2007 to early 2008 [*Vialard et al., 2008*]. The present study allows for resolution of this apparent paradox. The fact that some MJO events are associated with a chlorophyll bloom demonstrates that mixing with the subsurface occurred and that it, consequently, probably played a role in cooling the SST (as also suggested by *Vinayachandran and Saji [2008]*). However, we demonstrate in this study that Chl intraseasonal events, and hence the contribution of mixing/upwelling, are modulated by the thermocline depth, with larger events appearing when the thermocline is shallow in the SCTR but weaker events appearing otherwise. For example, the weak positive SLA during the December 2007 to January 2008 event directly observed by *Vialard et al. [2008]* might explain the relatively weak contribution of the mixing and upwelling for this event. When the thermocline is anomalously shallow, on the other hand, the atmospheric forcing will combine with vertical processes to produce stronger cooling and also a strong Chl response. It is also the modulation of the response by interannual variability which explains the relatively modest response of significant Chl intraseasonal

events in the SCTR (only 4 in 10 years; see Figure 8), while significant MJO-related atmospheric forcing events occur almost every year.

[38] **Acknowledgments.** We sincerely thank the NEMO system team for their development and maintenance of the NEMO ocean general circulation model. Support was provided by Vasco-Cirene (study of air-sea interactions in the Seychelles-Chagos thermocline ridge) and Toward Integration of Subgrid Turbulence in Ecosystem Dynamics (TWISTED) programs. J. Vialard did this work while hosted by the National Institute of Oceanography (Goa, India) as a visiting scientist. The Chl data were provided by the SeaWiFS Project and NASA's DAAC. QuikSCAT wind data were produced by Remote Sensing Systems (available at [www.remss.com](http://www.remss.com)) and were sponsored by the NASA Ocean Vector Winds Science Team.

## References

- Aumont, O., and L. Bopp (2006), Globalizing results from ocean in situ iron fertilization studies, *Global Biogeochem. Cycles*, *20*, GB2017, doi:10.1029/2005GB002591.
- Aumont, O., E. Maier-Reimer, S. Blain, and P. Monfray (2003), An ecosystem model of the global ocean including Fe, Si, P colimitations, *Global Biogeochem. Cycles*, *17*(2), 1060, doi:10.1029/2001GB001745.
- Balkanski, Y., M. Schulz, T. Claquin, C. Moulin, and P. Ginoux (2004), Global emissions of mineral aerosol: Formulation and validation using satellite imagery, in *Emissions of Atmospheric Trace Compounds*, edited by C. Granier, P. Artaxo, and C. E. Reeves, pp. 239–267, Kluwer Acad., Boston, Mass.
- Banse, K., and D. C. English (1993), Revision of satellite-based phytoplankton pigment data from the Arabian Sea during the northeast monsoon, *Mar. Res. Pakistan*, *2*, 83–103.
- Brock, J. C., and C. R. McClain (1992), Interannual variability in phytoplankton blooms observed in the northwestern Arabian Sea during the southwest monsoon, *J. Geophys. Res.*, *97*, 733–750.
- Cipollini, P., D. Cromwell, P. G. Challenor, and S. Raffaglio (2001), Rossby waves detected in global ocean colour data, *Geophys. Res. Lett.*, *28*, 323–326.
- Conkright, M. E., R. A. Locamini, H. E. Garcia, T. D. O'Brien, T. P. Boyer, C. Stephens, and J. Antonov (2002), World Ocean Atlas 2001: Objective analyses, data statistics and figures, CD-ROM documentation, *Natl. Oceanogr. Data Cent. Internal Rep.* *17*, 17 pp., Natl. Oceanogr. Data Cent., Silver Spring, Md.
- Dandonneau, Y., A. Vega, H. Loisel, Y. du Penhoat, and C. Menkes (2003), Oceanic Rossby waves acting as a “hay rake” for ecosystem floating by-products, *Science*, *302*, 1548–1551, doi:10.1126/science.1090729.
- de Boyer Montégut, C., G. Madec, A. S. Fischer, A. Lazar, and D. Iudicone (2004), Mixed layer depth over the global ocean: An examination of profile data and a profile-based climatology, *J. Geophys. Res.*, *109*, C12003, doi:10.1029/2004JC002378.
- de Boyer Montégut, C., J. Vialard, S. S. C. Shenoi, D. Shankar, F. Durand, C. Ethé, and G. Madec (2007), Simulated seasonal and interannual variability of mixed layer heat budget in the northern Indian Ocean, *J. Clim.*, *20*, 3249–3268, doi:10.1175/JCLI4148.1.
- Duvel, J. P., and J. Vialard (2007), Indo-Pacific sea surface temperature perturbations associated with intraseasonal oscillations of the tropical convection, *J. Clim.*, *20*, 3056–3082, doi:10.1175/JCLI4144.1.
- Duvel, J. P., R. Roca, and J. Vialard (2004), Ocean mixed layer temperature variations induced by intraseasonal convective perturbations over the Indian Ocean, *J. Atmos. Sci.*, *61*, 1004–1023.
- Geider, R. J., H. L. MacIntyre, and T. M. Kana (1998), A dynamic regulatory model of phytoplankton acclimation to light, nutrients and temperature, *Limnol. Oceanogr.*, *43*, 679–694.
- Gent, P. R., and J. C. McWilliams (1990), Isopycnal mixing in ocean circulation models, *J. Phys. Oceanogr.*, *20*, 150–155.
- Goose, H. (1997), Modelling the large-scale behaviour of the coupled ocean-sea-ice system, Ph.D. thesis, Univ. Cath. de Louvain, Louvain-La-Neuve, Belgium.
- Harrison, D. E., and G. A. Vecchi (1999), On the termination of El Niño, *Geophys. Res. Lett.*, *26*, 1593–1596.
- Harrison, D. E., and G. A. Vecchi (2001), January 1999 Indian Ocean cooling event, *Geophys. Res. Lett.*, *28*, 3717–3720.
- Hendon, H. (2005), Air-sea interaction, in *Intraseasonal Variability in the Atmosphere-Ocean Climate System*, edited by W. K. M. Lau and D. E. Waliser, pp. 223–246, Springer, Heidelberg, Germany.
- Hermes, J. C., and C. J. C. Reason (2008), Annual cycle of the South Indian Ocean (Seychelles-Chagos) thermocline ridge in a regional ocean model, *J. Geophys. Res.*, *113*, C04035, doi:10.1029/2007JC004363.
- Hood, R. R., K. E. Kohler, J. P. McCreary, and S. L. Smith (2003), A four-dimensional validation of a coupled physical-biological model of the Arabian Sea, *Deep Sea Res., Part II*, *50*, 2917–2945.
- Kawamiya, M. (2001), Mechanism of offshore nutrient supply in the western Arabian Sea, *J. Mar. Res.*, *59*, 675–696.
- Kawamiya, M., and A. Oschlies (2001), Formation of a basin-scale surface chlorophyll pattern by Rossby waves, *Geophys. Res. Lett.*, *28*, 4139–4142.
- Kawamiya, M., and A. Oschlies (2003), An eddy-permitting, coupled ecosystem-circulation model of the Arabian Sea: Comparison with observations, *J. Mar. Syst.*, *38*, 221–257.
- Koné, V., A. Aumont, M. Lévy, and L. Resplandy (2009), Physical and biogeochemical controls of the phytoplankton seasonal cycle in the Indian Ocean: A modeling study, *Geophys. Monogr. Ser.*, doi:10.1029/2008GM000700, in press.
- Large, W. G., and S. G. Yeager (2004), Diurnal to decadal global forcing for ocean and sea-ice models: The data sets and flux climatologies, *NCAR Tech. Note TN-460+STR*, 150 pp., Natl. Cent. for Atmos. Res., Boulder, Colo.
- Lévy, M., D. Shankar, J.-M. André, S. S. C. Shenoi, F. Durand, and C. de Boyer Montégut (2007), Basin-wide seasonal evolution of the Indian Ocean's phytoplankton blooms, *J. Geophys. Res.*, *112*, C12014, doi:10.1029/2007JC004090.
- Ludwig, W., J. L. Probst, and S. Kempe (1996), Predicting the oceanic input of organic carbon by continental erosion, *Global Biogeochem. Cycles*, *10*, 23–41.
- Madden, R. A., and P. R. Julian (1994), Observations of the 40–50 day tropical oscillation: A review, *Mon. Weather Rev.*, *122*, 814–837.
- Madec, G. (2008), NEMO ocean engine, *Note Pole Modelisation* *27*, 250 pp., Inst. Pierre et Simon Laplace, Paris, France.
- Masumoto, Y., and G. Meyers (1998), Forced Rossby waves in the southern tropical Indian Ocean, *J. Geophys. Res.*, *103*, 27,589–27,602.
- McCreary, J. P., Jr., P. K. Kundu, and R. Molinari (1993), A numerical investigation of dynamics, thermodynamics and mixed-layer processes in the Indian Ocean, *Prog. Oceanogr.*, *31*, 181–244.
- Middelburg, J. J., K. Soetaert, P. M. J. Herman, and C. Heip (1996), Denitrification in marine sediments: A model study, *Global Biogeochem. Cycles*, *10*, 661–673.
- Murtugudde, R., J. P. McCreary, and A. J. Busalacchi (2000), Oceanic processes associated with anomalous events in the Indian Ocean with relevance to 1997–1998, *J. Geophys. Res.*, *105*, 3295–3306.
- Prasanna Kumar, S., M. Nuncio, J. Narvekar, A. Kumar, S. Sardesai, S. N. de Souza, M. Gauns, N. Ramaiah, and M. Madhupratap (2004), Are eddies nature's trigger to enhance biological productivity in the Bay of Bengal?, *Geophys. Res. Lett.*, *31*, L07309, doi:10.1029/2003GL019274.
- Rao, S. A., and S. K. Behera (2005), Subsurface influence on SST in the tropical Indian Ocean: Structure and interannual variability, *Dyn. Atmos. Oceans*, *39*, 103–135.
- Rossov, W. B., and R. A. Schiffer (1999), Advances in understanding clouds from ISCCP, *Bull. Am. Meteorol. Soc.*, *80*, 2261–2288.
- Saji, N. H., B. N. Goswami, P. N. Vinayachandran, and T. Yamagata (1999), A dipole mode in the tropical Indian Ocean, *Nature*, *401*, 360–363.
- Saji, N. H., S.-P. Xie, and C.-Y. Tam (2006), Satellite observations of intense intraseasonal cooling events in the tropical south Indian Ocean, *Geophys. Res. Lett.*, *33*, L14704, doi:10.1029/2006GL026525.
- Schott, F., and J. P. McCreary (2001), The monsoon circulation of the Indian Ocean, *Prog. Oceanogr.*, *51*, 1–123.
- Smith, S. L., L. A. Codispoti, J. M. Morrison, and R. T. Barber (1998), The 1994–1996 Arabian Sea Expedition: An integrated, interdisciplinary investigation of the response of the northwestern Indian Ocean to monsoonal forcing, *Deep Sea Res., Part II*, *45*, 1905–1915.
- Takahashi, T., W. S. Broecker, and S. Langer (1985), Refield ratio based on chemical data from isopycnal surfaces, *J. Geophys. Res.*, *90*, 6907–6924.
- Trenberth, K. E., J. G. Olson, and W. G. Large (1989), A global ocean wind stress climatology based on the ECMWF analyses, *NCAR Tech. Note NCAR/TN-338+STR*, 93 pp., Natl. Cent. for Atmos. Res., Boulder, Colo.
- Uppala, S. M., et al. (2005), The ERA-40 re-analysis, *Q. J. R. Meteorol. Soc.*, *131*, 2961–3012.
- Uz, B. M., J. A. Yoder, and V. Osychny (2001), Pumping of nutrients to ocean surface waters by the action of propagating planetary waves, *Nature*, *409*, 597–600.
- Vialard, J., G. Foltz, M. McPhaden, J.-P. Duvel, and C. de Boyer Montégut (2008), Strong Indian Ocean sea surface temperature signals associated with the Madden-Julian Oscillation in late 2007 and early 2008, *Geophys. Res. Lett.*, *35*, L19608, doi:10.1029/2008GL035238.
- Vialard, J., et al. (2009), Cirene: Air-sea interactions in the Seychelles-Chagos thermocline ridge region, *Bull. Am. Meteorol. Soc.*, *90*, 45–61.

- Vinayachandran, P. N., and N. H. Saji (2008), Mechanisms of South Indian Ocean intraseasonal cooling, *Geophys. Res. Lett.*, *35*, L23607, doi:10.1029/2008GL035733.
- Waliser, D. E., R. Murtugudde, and L. Lucas (2003), Indo-Pacific Ocean response to atmospheric intraseasonal variability: 1. Austral summer and the Madden-Julian Oscillation, *J. Geophys. Res.*, *108*(C5), 3160, doi:10.1029/2002JC001620.
- Waliser, D. E., R. Murtugudde, and L. E. Lucas (2004), Indo-Pacific Ocean response to atmospheric intraseasonal variability: 2. Boreal summer and the intraseasonal oscillation, *J. Geophys. Res.*, *109*, C03030, doi:10.1029/2003JC002002.
- Waliser, D. E., R. Murtugudde, P. Strutton, and J.-L. Li (2005), Subseasonal organization of ocean chlorophyll: Prospects for prediction based on the Madden-Julian Oscillation, *Geophys. Res. Lett.*, *32*, L23602, 10.1029/2005GL024300.
- Webster, P. J., A. M. Moore, J. P. Loschnigg, and R. R. Leben (1999), Coupled oceanic-atmospheric dynamics in the Indian Ocean during 1997–98, *Nature*, *401*, 356–360.
- Wheeler, M., and H. Hendon (2004), An all-season real-time multivariate MJO index: Development of an index for monitoring and prediction, *Mon. Weather Rev.*, *132*, 1917–1932.
- Wiggert, J. D., B. H. Jones, T. D. Dickey, K. H. Brink, R. A. Weller, J. Marra, and L. A. Codispoti (2000), The northeast monsoon's impact on mixing, phytoplankton biomass and nutrient cycling in the Arabian Sea, *Deep Sea Res., Part II*, *47*, 1353–1385.
- Wiggert, J. D., R. G. Murtugudde, and C. R. McClain (2002), Processes controlling interannual variations in wintertime (northeast monsoon) primary productivity in the central Arabian Sea, *Deep Sea Res., Part II*, *49*, 2319–2343.
- Wiggert, J. D., R. R. Hood, K. Banse, and J. C. Kindle (2005), Monsoon-driven biogeochemical processes in the Arabian Sea, *Prog. Oceanogr.*, *65*, 176–213.
- Wiggert, J. D., R. Murtugudde, and J. R. Christian (2006), Annual ecosystem variability in the tropical Indian Ocean: Results of a coupled biophysical ocean general circulation model, *Deep Sea Res., Part II*, *53*, 644–676.
- Xie, S.-P., H. Annamalai, F. A. Schott, and J. P. McCreary (2002), Structure and mechanisms of south Indian Ocean climate variability, *J. Clim.*, *15*, 864–878.
- Yokoi, T., T. Tozuka, and T. Yamagata (2008), Seasonal variation of the Seychelles Dome, *J. Clim.*, *21*, 3740–3754.
- Yu, W., B. Xiang, L. Liu, and N. Liu (2005), Understanding the origins of interannual thermocline variations in the tropical Indian Ocean, *Geophys. Res. Lett.*, *32*, L24706, doi:10.1029/2005GL024327.
- Zhang, C. (2005), Madden-Julian Oscillation, *Rev. Geophys.*, *43*, RG2003, doi:10.1029/2004RG000158.

---

O. Aumont, LPO, IRD, IFREMER, UBO, CNRS, F-29200 Brest, France.  
Y. Dandonneau, M. Lévy, L. Resplandy, and J. Vialard, LOCEAN-IPSL, IRD, MNHN, UPMC, CNRS, BC100, 4 place Jussieu, F-75252 Paris CEDEX 05, France. (lrld@locean-ipsl.upmc.fr)